**Title:** Distinct networks coupled with parietal cortex for spatial representations inside and outside the visual field

**Authors:** Bo Zhang [1, 3, 4], Fan Wang [7,8,9], Qi Zhang [1, 10], Naya Yuji [1, 2, 5, 6, *]

**Affiliations:**

[1] School of Psychological and Cognitive Sciences, Peking University, No. 52, Haidian Road, Haidian District, Beijing 100805, China

[2] IDG/McGovern Institute for Brain Research at Peking University, No. 52, Haidian Road, Haidian District, Beijing 100805, China

[3] Beijing Academy of Artificial Intelligence, Beijing, 100084, China

[4] Tsinghua Laboratory of Brain and Intelligence, 160 Chengfu Rd., SanCaiTang Building, Haidian District, Beijing, 100084, China

[5] Center for Life Sciences, Peking University, No. 52, Haidian Road, Haidian District, Beijing 100805, China

[6] Beijing Key Laboratory of Behavior and Mental Health, Peking University, No. 52, Haidian Road, Haidian District, Beijing 100805, China

[7] State Key Laboratory of Brain and Cognitive Science, Institute of Biophysics, Chinese Academy of Sciences, 15 Datun Road, Beijing 100101, China

[8] CAS Center for Excellence in Brain Science and Intelligence Technology

[9] University of Chinese Academy of Sciences, 19A Yuquan Road, Beijing 100049, China

[10] Fujian Key Laboratory of Applied Cognition and Personality, School of Educational Science, Minnan Normal University, 36 Xianqianzhi Street, Zhangzhou 363000, China

**Corresponding author:** Yuji Naya

Address: School of Psychological and Cognitive Sciences, Peking University, No. 52, Haidian Road, Wang Kezhen Building, Room 1707,Haidian District, Beijing 100805, China

E-mail: yujin@pku.edu.cn

**Conflict of interest statement**: No competing financial interests

**Acknowledgments:** This work was supported by the National Natural Science Foundation of China Grant 31421003 (to Y.N.) and by the Fundamental Research Funds for the Central Universities, PKU (7100602954 to Y.N.). We thank the National Center for Protein Sciences at Peking University for assistance with MRI data collection, and the State Key Laboratory of Brain and Cognitive Science at the Chinese Academy of Sciences for assistance with MEG scanning, which was supported in part by grants from the Ministry of Science and Technology of China (2019YFA0707103), National Nature Science Foundation of China (31730039), and Strategic Priority Research Program of the Chinese Academy of Science (XDB32010300). Computational work was supported by resources provided by the High-performance Computing Platform of Peking University.

## Abstract

Our mental representation of egocentric space is influenced by the disproportionate sensory perception of the body. Previous studies have focused on the neural architecture for egocentric representations within the visual field. However, the space representation underlying the body is still unclear. To address this problem, we applied both fMRI and MEG to a spatial-memory paradigm by using a virtual environment in which human participants remembered a target location left, right, or back relative to their own body. Both experiments showed larger involvement of the frontoparietal network in representing a retrieved target on the left/right side than on the back. Conversely, the medial temporal lobe (MTL)-parietal network was more involved in retrieving a target behind the participants. The MEG data showed preferential connectivity in the alpha-band frequency in both networks. These findings suggest that the parietal cortex may represent the entire space around the self-body by coordinating two distinct brain networks.

## Introduction

While planning to reach a target, it is necessary to obtain its location information in the body-centered reference frame or the so-called "egocentric" spatial coordinates[1-4]. Previous studies using humans and nonhuman primates indicated the crucial involvement of the parietal cortex in the representation of egocentric location for sensory perception, motor action, and their coordination[4-10]. Anatomically, the parietal cortex is located at the late stage of the dorsal pathway, which is often named the "where" or "how" pathway[11-12]. Perceptual signals, including visual, somatosensory, and vestibular information, converge on the parietal cortex, which interacts with the frontal eye field (FEF), the region associated with attention and eye movement toward a target in the external space around the self-body[13-16]. These anatomical connection patterns are consistent with those reported by neuropsychological studies, that is, damage to the parietal cortex results in a form of impaired egocentric spatial awareness known as hemispherical neglect, which leads to neglect of a target on one side of the field of vision[17]. Hemispherical neglect appears not only in perception but also in the memory field, where it is known as "representational neglect"[18]. On the basis of data accumulated from human imaging studies examining spatial navigation and episodic recollection[19-23], the parietal cortex is considered to represent the egocentric space for both perception and memory.

Mnemonic representations of the egocentric space raise the question of whether the spatial representation differs between the inside and outside of a visual field. While the former can be represented in both vision and memory, the latter can be represented only in memory. Previous human behavioral studies reported decreased performance[24] or prolonged response latency[25] when participants located a target behind them. This phenomenon, known as the "alignment effect"[26] or "front facilitation,"[27] suggests that the space surrounding our body is coded heterogeneously by different neural systems depending on the target location

along the anterior-posterior axis of the self-body[27]. To explore the neural architectures responsible for the representation of egocentric space, previous studies mostly examined the target representation within the visual field; however, one neuroimaging study, which examined target representation retrieved from memory, suggested that the parietal cortex codes the whole space around the self-body[28]. However, the representation properties of the inside/outside of the visual field in the parietal cortex and its interactions with associated brain areas remain unsolved.

To characterize the neural architectures supporting the mental representations of egocentric space inside and outside the visual field, we applied functional magnetic resonance imaging (fMRI) and magnetoencephalography (MEG) to a spatial-memory paradigm using a 3D virtual environment for human participants (Fig. 1a), which we recently devised[29]. In this paradigm, participants encoded a spatial relationship among three objects (walking period) in each trial. While the same three objects were used across trials, their spatial relationships differed pseudorandomly. After the walking period, one of the three objects was presented in the center of the display with the environmental background, which prompted the participants to feel as if they were facing the objects in the virtual environment (facing period)[29]. Then, one of the other two objects was presented on a scrambled background as the target object (targeting period). The participants remembered the location of the target object relative to the body. The to-be-remembered targeting locations could be in the left, right, or back positions of the participants' egocentric spaces (Fig. 1b). This spatial-memory paradigm allowed us to compare the neural representations of egocentric space between the inside and outside of the visual field when the participants remembered a target location, which had been encoded in each trial.

# Results

**Behavioral performance**

Nineteen and 12 healthy volunteers participated in the fMRI and MEG experiments, respectively. The participants performed the spatial-memory task with high accuracy rates in both the experiments (MRI: 93.6% ± 1.5%; MEG: 90.4% ± 1.9%). The performances did not differ among the three target locations (i.e., right, left, and back) in both fMRI [$F$ (2,54) = 0.82, $P$ = 0.44] and MEG [$F$ (2,33) = 0.08, $P$ = 0.93] experiments (Fig. 2a), indicating that the participants solved the spatial memory task accurately regardless of the target location.

**MRI contrast analysis**

The neural activity in the fMRI experiment was examined using the 4-s time-window of the targeting period in which the participants remembered the location of the target object (i.e., human character) relative to their self-body in the virtual environment. A contrast analysis showed a significantly stronger blood-oxygen-level-dependent (BOLD) signal for the left/right-target condition than for the back-target condition in the parietal cortex, precuneus, FEF, and SMA (Fig. 3a, $P < 0.01$; initial threshold, $P < 0.05$; cluster-corrected for multiple comparisons). In contrast, no brain areas showed a significantly stronger BOLD signal for the back-target condition than for the left/right-target condition in the same statistical condition with multiple comparisons, although we found a significant cluster for the back-target location in the right rhinal cortex (entorhinal cortex [ERC] and perirhinal cortex [PRC]) of the MTL when we used a more liberal threshold (Fig. 3b, $P < 0.05$, uncorrected).

Regarding the larger activation of the dorsal brain regions under the left/right-target conditions than the back-target condition, one question might be whether the elevated activities can be explained by eye movements under different target conditions. To test this possibility, we examined the participants' gaze positions during the 4-s time window of the targeting period. The gaze positions did not differ among the egocentric locations of the

124 retrieved targets in the horizontal direction [$F$ (2, 51) = 1.7, $P$ = 0.19] or the vertical direction
125 [$F$ (2, 51) = 0.084, $P$ = 0.92] (Fig. 2b). In addition to the average gaze position, we examined
126 the frequencies of saccadic eye movements (see Methods), but no significant difference was
127 found between the left/right and back-target conditions during the targeting period [$F$ (2, 51)
128 = 0.007, $P$ = 0.99] (Fig. 2c). These results indicate that the increased activity in the dorsal
129 brain regions was not due to eye movements that may have been induced by the retrieved
130 egocentric locations. Taken together, these findings reasonably suggest that the frontoparietal
131 cortical areas were involved in an additional mental process to represent a retrieved target to
132 the left/right in comparison with that behind the participants' self-body. Similarly,
133 remembering a target behind the self-body may employ the right MTL more than when the
134 participants remembered a target to their left/right.

135 **MRI functional-connectivity analysis**

136 We subsequently investigated the brain regions that interacted with the parietal cortex and
137 precuneus when the participants remembered the target location to their left, right, and back.
138 To examine the interactions, we conducted whole-brain functional connectivity analysis
139 using the anatomical ROIs of the parietal cortex and precuneus as the seeds based on the
140 AAL (see Methods for details). The results showed that, in addition to a mutual connectivity
141 between these brain areas, both the parietal cortex and precuneus exhibited a significantly
142 higher connectivity to the FEF and SMA under the left/right-target condition than under the
143 back-target condition (Fig. 4a, $P < 0.01$, initial threshold, $P < 0.05$, cluster-corrected for
144 multiple comparison). This result indicates the cooperative involvement of the FEF, SMA,
145 parietal cortex, and precuneus while processing a target object in the visual field, even when
146 the egocentric object location was not perceived. In contrast, the parietal cortex, but not the
147 precuneus, showed increased functional connectivity to the right ERC when a retrieved target
148 location was behind the participants' body (Fig. 4b, $P < 0.01$, initial threshold, $P < 0.05$,

149 cluster-corrected for multiple comparisons via small-volume correction using the bilateral
150 MTL mask). We also examined the functional connectivity using FEF and SMA seeds and
151 found that these two brain regions exhibited strong connectivity to the parietal cortex and
152 precuneus in the left/right-target condition but did not show increased functional connectivity
153 to any other brain regions, including the ERC, in the back-target condition. These results
154 suggest that our egocentric space is represented by two distinct brain networks: the
155 frontoparietal network for the target within the visual field, and the MTL-parietal network for
156 the target outside the visual field.

157 **MEG contrast analysis**

158 The fMRI experiments showed preferential involvement of the frontoparietal network in the
159 left/right-target condition and those of the MTL-parietal network in the back-target condition.
160 To examine the temporal dynamics of these brain networks, we subsequently conducted an
161 MEG study using the same spatial memory task that was used for the fMRI study, except for
162 the time parameters (Fig. 1a).

163 Figure 5a shows the results of the contrast analysis that compared the activity strength
164 at each sensor between the left/right-target and back-target conditions. We found a cluster of
165 sensors in the left-posterior area, which showed significantly stronger activity under the
166 left/right-target condition than under the back-target condition during 0.67–0.85 s after the
167 onset of the targeting period ($P < 0.05$, initial threshold, two tailed; $P = 0.04$, spatial-temporal
168 cluster-corrected for multiple comparison) (Fig. 5b). Conversely, no cluster of sensors
169 showed stronger activity under the back-target condition than under the left/right-target
170 condition. In addition to the fMRI study, we examined the participants' gaze positions and
171 frequencies of saccadic eye movements in MEG experiments. There was no significant
172 difference among the left, right, and back target conditions during the 1-s time-window of the
173 targeting period in the eye positions [$F$ (2, 27) = 0.32, 0.42, $P = 0.73$ and 0.66, respectively,

174 for the horizontal and vertical positions, respectively] (Fig. 2b) nor the saccade frequencies
175 [$F$ (2, 27) = 0.14, $P$ = 0.87] (Fig. 2c). These results were consistent with the results of the
176 fMRI experiments, indicating predominant spatial representation processing within the visual
177 field relative to that outside the visual field.

178 To examine the changes in neural activity required for the retrieval of a target
179 location, we compared the activity strength under back-target, left-target, and right-target
180 conditions with the control trials, in which a targeting-character was not presented and the
181 participants were not required to remember a target location (Fig. 5c). Figure 5d shows the
182 time course of the topographic activity map under each condition relative to that under
183 control conditions. Increased activity was observed in the left posterior area of the head. This
184 left-posterior cluster showed a significant increase in activity during 0.5–0.6 s from the onset
185 of the targeting period under the left-target and right-target conditions ($P < 0.05$, initial
186 threshold; $P < 0.05$, cluster-corrected for multiple comparison) although the same trend of
187 increase in activity was observed under the back-target condition [$t(11) = 2.42$, $P = 0.03$,
188 uncorrected]. To localize the brain regions contributing to the significant activity increase in
189 the left-posterior cluster, we conducted a source analysis of the MEG signal[30]. The source
190 powers were distributed largely in the parietal cortex and precuneus in the left- and right-
191 target conditions (Fig. 5e). We also found that the source power for the back-target condition
192 was distributed in the parietal cortex and precuneus, although the level of source power was
193 smaller than those under the left -and right-target conditions.

194 To explore the brain regions exhibiting larger neural activity under the back-target
195 condition than under the left/right-target condition, we conducted a whole-brain analysis to
196 compare the source power between the two conditions at intervals of 0.2 s after the onset of
197 the targeting period (Fig. 6a). We found a strong source-power for the back-target condition
198 in the right MTL, including the ERC, during 0.2–0.4 s after the onset of the targeting period.

199 Using anatomical ROIs of each hemisphere of the whole MTL, we examined the precise time
200 courses of the source power for the back -and left/right-target conditions relative to the
201 control trials. The results indicated elevations in the source power after the onset of the
202 targeting period under both back-target and left/right-target conditions in both hemispheres of
203 the MTL. However, only the right MTL exhibited a significantly larger source power for the
204 back-target condition than for the left/right-target condition in the early phase (0.25–0.37 s)
205 after the onset of the targeting period (Fig. 6b, $P < 0.05$, initial threshold; $P < 0.05$, spatial-
206 temporal cluster correction for multiple comparison, two-tailed). We further examined the
207 source power in the right MTL by using the anatomical masks of its subregions and found
208 that the source power was larger under the back-target condition than under the left/right-
209 target condition in all the subregions [HPC: $t(11) = 3.00$, $P = 0.048$; PHC: $t(11) = 2.98$, $P =$
210 $0.049$; PRC: $t(11) = 3.22$, $P = 0.032$; ERC: $t(11) = 3.39$, $P = 0.024$, Bonferroni-corrected for
211 multiple comparisons (n = 4)] (Fig. 6c). Collectively, the MEG contrast analyses in source-
212 power between the back- and left/right-target conditions indicate that the right MTL,
213 including the ERC, was involved more in the back-target condition than in the left/right-
214 target condition in the early phase (0.25–0.37 s) after the onset of the targeting period, while
215 the parietal cortex and precuneus were involved more in the left/right-target condition than in
216 the back-target condition in the late phase (Fig. 5b, 0.67–0.85 s).

217 **MEG functional-connectivity analysis**

218 Next, we examined the connectivity of the parietal cortex with the FEF, SMA, and MTL
219 areas by calculating the phase lag index (PLI) for the MEG data[31-32]. We chose the two time-
220 windows of interest (0.08–0.48 s and 0.56–0.96 s after the onset of targeting period, see
221 method for details) since they could include at least three cycles of alpha-band waves and
222 cover the early and late phases, which were revealed from the MEG contrast analysis (Figs.
223 5&6). Figure 7 shows the differences in connectivity between the back- and left/right-target

conditions. The connectivity patterns differed significantly between the two time windows in the alpha band (8–13 Hz) [$F$ (1, 132) = 8.24, $P$ = 0.02, repeated-measures two-way ANOVA, Bonferroni-corrected for multiple comparisons, n = 4 for frequency bands], but not in the other bands. During the early time window, the parietal cortex showed a larger connectivity with the right ERC and PRC of the MTL under the back-target condition than under the left/right-target condition, although the difference was statistically marginal [ERC: $t$(11) = 2.16, $P$ = 0.06; PRC: $t$(11) = 1.91, $P$ = 0.08, uncorrected]. Conversely, we found a larger connectivity of the parietal cortex with the FEF [$t$(11) = 2.61, $P$ = 0.02, uncorrected] and SMA [$t$(11) = 1.73, $P$ = 0.11, uncorrected] under the left/right-target condition than under the back-target condition during the late time window. These results were consistent with those obtained with functional connectivity analysis using fMRI (Fig. 4). In contrast to the time-dependent alpha-band connectivity of the parietal cortex to the MTL and frontal areas, we did not find a change in the connectivity of the precuneus with any of the ROIs in any frequency band across the two time windows of interest.

## Discussion

The present combined fMRI and MEG study showed greater involvement of the fronto-parietal network when a participant remembered a target location on the left/right side than on the back of the self-body. Conversely, larger involvement of the MTL-parietal network was revealed when a target object was behind a participant. These results suggest that the parietal cortex represents the external space surrounding the self-body in mind by interacting with the dorsal frontal regions and the MTL.

A previous human fMRI study using multi-voxel pattern analysis (MVPA) reported that the parietal cortex codes the egocentric space both inside and outside the visual field[28], which is consistent with the findings of our previous MVPA-based study that employed the same spatial-memory task as the present one[29]. However, Schindler and Barteles[28] did not find the relationship between BOLD signal strength and egocentric space demonstrated by the present study. One reason for this discrepancy might be the different types of memory required for the two studies. Schindler and Barteles[28] intensively trained participants to learn a fixed spatial arrangement of eight objects for several days before the MRI scans. During the scans, the participants remembered a target object location based on the knowledge that they stored as long-term memory in a different room. In contrast, the present study prompted the participants to encode a trial-specific spatial relationship among the three objects in each trial (see Methods) and remember a target location from their short-term memory in the same 3D virtual environment as they encoded during the scan. These different task conditions may have resulted in different participant retrieval strategies between the two studies, which may have affected space representations in the parietal cortex.

The present study exhibited disproportional spatial representations around the self-body, with a bias toward the left/right-target location in comparison with the back-target location. The preferential processing of the left/right-target location relative to the back by

263 the frontoparietal network is consistent with the results of previous behavioral studies that
264 reported "front facilitation," i.e., the location of a target in the anterior part of a participant is
265 more efficiently detected than a target located behind them[24,25,27]. On the other hand, we
266 found greater involvement of the MTL-parietal network in representing the back target
267 location than the left/right target location. Interestingly, the present MEG experiment
268 comparing each target-location condition with the control condition showed that the source
269 power increased in the MTL not only for the back-target location but also for the left/right-
270 target location (Figs. 6b). These results suggest that the retrieved target location information
271 is transmitted from the MTL to the parietal cortex regardless of whether the location was
272 inside or outside the visual field. These findings are consistent with the results of previous
273 studies that suggested the involvement of both the MTL and parietal cortex as members of
274 the core brain system in the recollection of episodic memory[33,34]. We hypothesized that the
275 MTL-parietal network was involved in the back-target condition more than the left/right-
276 target condition to generate a mental representation of a retrieved target location because the
277 representation in the left/right-target condition was also supported by the frontoparietal
278 network, which might reduce the demand on the MTL-parietal network in comparison with
279 the back-target condition.

280 While the fMRI experiment suggested the preferential involvement of only the rhinal
281 cortex, particularly the ERC in the back-target condition, the MEG experiment suggested the
282 involvement of all MTL subareas. This inconsistency might be due to the ill-posed nature of
283 the MEG inverse problem (e.g., the "source leakage"), since a limited number of magnetic-
284 field sensors yielded insufficient activity to discriminate among thousands of source points,
285 particularly for neighboring regions[35-37]. The MEG source power in the other MTL
286 subregions might thus be caused by signal leakage from the ERC. Another possibility might
287 be that the MEG signal reflected synchronized activity at each instantaneous time point and

288 would be more sensitive to transient neuronal operations than fMRI analysis, which is based
289 on the averaged BOLD signal[38] in each TR (2 s). In either case, the ERC might play a key
290 role in the MTL-parietal network for the representation of a retrieved target location, which is
291 consistent with the results of previous studies that examined the spatial properties of the ERC
292 neurons (e.g., grid cells, head direction cells) in both rodents[22,39-42] and primates[43-45].
293 Importantly, the primate ERC reportedly represents the external space according to the gaze
294 position and even in imagined navigation[46]. In contrast to the ERC, other MTL subregions
295 may be involved in the retrieval of the target location[47-49]. Considering the high performance
296 of the present spatial memory task and the fact that post-scan interviews of the participants
297 showed no strategic efforts for retrieval, the retrieval process might be only transient in the
298 present experimental paradigm, which could be detected more efficiently by MEG than by
299 fMRI.

300 The MEG connectivity analysis using PLI revealed a preferential increase in
301 synchronization at alpha-band frequency (8–13 Hz) for both frontoparietal and MTL-parietal
302 networks for the left/right-target and back-target conditions, respectively. In contrast, we did
303 not observe a differential increase in synchronization in the other frequency bands. These
304 findings were consistent with the results of previous MEG and EEG studies, which suggested
305 functional roles of alpha-band phase synchrony in long-range communications across distant
306 brain regions, including the parietal cortex[8,50-53]. One remaining question concerns the
307 functional significance of the MTL-parietal network in daily life. In the present spatial-
308 memory paradigm, the participants obtained the egocentric target location from their short-
309 term memory, either inside or outside the visual field[29]. Instead, we usually locate a target
310 inside the visual field for a subsequent action by looking at it[54,55], while we occasionally
311 retrieve a target behind us from short-term memory. Therefore, the visual modality of
312 information on the back is always encoded in the past, and the preceding spatiotemporal

information is retained in the MTL[56,57]. Collectively, the parietal cortex may represent the whole space around the self-body by coordinating the MTL-parietal network and the frontoparietal network, which may equip us with the mental representation of the present external world interacting with our past (retrieval) and future (action planning).

## Materials and Methods

### Participants

Nineteen and 12 right-handed university students with normal or corrected-to-normal vision were recruited from Peking University for fMRI and MEG experiments, respectively (fMRI: 12 women, 7 men; MEG: 4 women, 8 men). The average age of the participants recruited for the fMRI and MEG experiments was 24.9 years (range: 18–30 years) and 22.5 years (range: 19–25 years), respectively. None of the participants had a history of psychiatric or neurological disorders; all of them provided written informed consent prior to the start of the experiment, which was approved by the Research Ethics Committee of Peking University.

### Experimental design

*Experimental design:* The details of the study design have been described previously[29]. A 3D virtual environment was programmed using the Unity platform (Unity Technologies, San Francisco). Three animated 3D human characters (Mixamo, San Francisco, https://www.mixamo.com) were placed on three out of four locations pseudo-randomly across trials (Fig. 1a). Participants performed the task using a first-person perspective with a 90° field of view (aspect ratio = 4:3) and had never seen a top-down view of the virtual environment. Experimental stimuli were presented through an LCD projector with a resolution of 1024 × 768 pixels.

The spatial memory task included 144 and 72 trials in the MRI and MEG experiments, respectively. In each trial, participants walked from one of the four starting locations toward the human characters and stopped on the wood plate in the center of the environment. After the walking period, participants experienced a “facing period” and a “targeting period” sequentially. In the facing period, one of the human characters was

342 presented as a facing-character in the center of the display with the environmental
343 background for 2.0 s (MRI) or 1.0 s (MEG), with the other two characters being invisible. In
344 the targeting period, a photo of one of the remaining characters (named as the "targeting-
345 character") was presented as a target on a scrambled background for 2.0 s (MRI) or 1.0 s
346 (MEG). Each of the three periods was followed by a 2.0-s (MRI) or 1.0-s (MEG) delay (noise
347 screen). At the end of each trial, participants indicated the direction of the target relative to
348 their self-body by pressing a button when a cue was presented.

349 We added head-nodding detection (HND) trials (16 trials for MRI and 36 trials for
350 MEG) to the spatial memory task. In the HND trials, a photo of one of the human characters
351 was presented after the walking period, and the participants were then asked to indicate
352 whether the human character nodded its head during the walking period. Each human
353 character nodded its head at a probability of 20.6% at a random time point between the start
354 and end of walking. Because the trial types were indistinguishable during the walking period,
355 the participants were required to pay attention to the head-nodding of the human characters
356 during the walking period, which would reduce the possibility of voluntary memorization of
357 the spatial relationship of the three objects. Post-scanning interviews showed that none of the
358 participants made efforts to memorize the spatial relationship[29].

359 *MEG control conditions:* Two control conditions (36 trials for each) were added to the spatial
360 memory task in the MEG experiment. In the control conditions, after the walking period, a
361 white cross was presented instead of a human character during both the facing and targeting
362 periods or during the targeting period (Fig. 4c). The participants were instructed to rest with
363 their eyes open and fixate on the white cross. After the targeting period, the participants
364 pressed a button corresponding to the number presented on the screen during the response
365 period. The number was determined randomly from one to four in each trial of the control
366 conditions.

367

368 **fMRI acquisition and analysis**

369 *MRI scanning parameters:* BOLD MRI images were acquired using a 3T Siemens Prisma
370 scanner equipped with a 20-channel receiver head coil. Functional data were acquired with a
371 multi-band echo planar imaging sequence (TR: 2000 ms; TE: 30 ms; matrix size: 112 × 112 ×
372 62; flip angle: 90°; gap: 0.3 mm; resolution: 2 × 2 × 2.3 $mm^3$; number of slices: 62; slice
373 thickness: 2 mm; gap between slices: 0.3 mm; slice orientation: transversal). The signals of
374 the original voxels (i.e., 2 × 2 × 2 $mm^3$) were assigned to the corresponding voxels without a
375 gap (2 × 2 × 2.3 $mm^3$) to construct participants' native space images. Four experimental
376 sessions were conducted with 478, 476, 473, and 475 of TRs on average. A high-resolution
377 T1-weighted three-dimensional anatomical data set was collected to facilitate registration
378 (MPRAGE: TR: 2530 ms; TE: 2.98 ms; matrix size: 448 × 512 × 192; flip angle: 7°;
379 resolution: 0.5 × 0.5 × 1 $mm^3$; number of slices: 192; slice thickness: 1 mm; slice orientation:
380 sagittal).

381 *fMRI preprocessing:* BOLD images of each scanning session were preprocessed
382 independently using FSL FEAT (FMRIB's Software Library, version 6.00,
383 https://fsl.fmrib.ox.ac.uk/fsl/fslwiki)[58,59]. For each session, the first three functional volumes
384 were discarded to allow for T1 equilibration, and the remaining functional volumes were
385 slice-time corrected, realigned to the first image, high-pass filtered at 100 s, and smoothed
386 using a 5-mm FWHM Gaussian filter.

387 *Univariate analysis:* The 4-s BOLD signals of the targeting period were modeled using
388 univariate general linear models (GLM) with the three egocentric directions (left, right, and
389 back) included as regressors in each experimental session (40 trials) for each participant. The
390 BOLD signals in the other task periods were modeled by additional regressors, including 12
391 visual patterns for the 8-s walking period (three spatial arrangements of human characters ×

392 four walking directions), the four types of body rotation for the 4-s facing period (135° and
393 45° in the clockwise and anti-clockwise directions), the three buttons that participants pressed
394 during their response for the response period, the time period for the HND trials, and the six
395 motion parameters. A canonical hemodynamic response function was used for each task
396 period in GLM. This procedure generated a parameter map for each of the three egocentric
397 directions (left, right, and back). The parameter maps were averaged across four scanning
398 sessions for each egocentric direction and registered to a T1-weighted standard image
399 (MNI152) using FSL FLIRT[60,61] before group-level statistical analyses. The voxel size was
400 converted into a 2 × 2 × 2 $mm^3$ resolution during the registration process.
401 *Connectivity analysis:* To conduct whole-brain analyses examining the functional
402 connectivity of the parietal cortex and precuneus, we first removed several sources of
403 spurious variance along with their temporal derivatives from the preprocessed functional data
404 by performing a GLM, which included (1) the mean time courses of the BOLD signal across
405 voxels within the lateral ventricles; (2) white matter; (3) whole brain; and (4) the six motion
406 parameters as regressors. The residual signals were bandpass-filtered, leaving signals within
407 the frequency range of 0.01–0.1 Hz and shifted by two TR intervals (4 s)[62-64]. The signals in
408 the participant's native space were registered to a T1-weighted standard image (MNI152)
409 using FSL FLIRT[60,61]. Then, we extracted the TRs during the 4-s targeting period from each
410 trial and concatenated them with those in the next trial for each of the three egocentric
411 directions and each session. The BOLD signals in each voxel were z-transformed along the
412 time course for each direction. Next, we averaged the z-transformed BOLD signals over the
413 anatomical masks of the brain areas (i.e., the seeds of the parietal cortex and precuneus) on
414 the basis of the automated anatomical labeling (AAL) template[65], which generated a regional
415 time course across trials for each egocentric direction in a session[66]. The regional time course
416 of each seed was then correlated with the time course of each voxel in the whole brain, which

417 yielded a whole-brain correlation map for the left-, right-, and back-target conditions
418 separately. The correlation maps were averaged across four scanning sessions (and left-and
419 right-target conditions) before submitting them to a group-level statistical analysis.
420
421 **MEG acquisition and analysis**
422 *MEG scanning parameters:* Neuromagnetic signals were recorded with a 275-channel whole-
423 head axial gradiometer DSQ-3500 MEG system (CTF MEG, Canada) at a sampling rate of
424 1200 Hz. A third-order synthetic gradiometer and linear drift corrections were applied to
425 remove far-field noise. To measure the head position within the MEG helmet, three head-
426 position indicator (HPI) coils were attached to the nasion and two preauricular points of each
427 participant to coregister their head position with the sensor coordinate system. During
428 scanning, customized chin-rest equipment compatible with MEG was prepared to ensure that
429 head movements did not exceed 2 mm. After MEG recording, each participant underwent
430 anatomical MRI scans on a 3T Siemens Prisma scanner (voxel size: 1 $mm^3$; flip angle: 9°;
431 TE: 1.97 ms; TR: 2,300 ms; field of view: 256 × 256 × 176 $mm^3$), and three MRI markers
432 were attached to the locations of the HPI coils to align each participant's anatomical image to
433 the MEG sensor positions.
434 *MEG preprocessing:* Raw signals from the MEG experiment were preprocessed and analyzed
435 using the MNE Python toolbox (v0.19; available at: https://mne.tools/stable/index.html)[67,68].
436 The time courses of the MEG signal were bandpass-filtered between 1 and 100 Hz offline.
437 Artifacts (e.g., eye movements, eye blinks, and cardiac movements) were removed by
438 performing independent component analysis (ICA). Then, the MEG signals were visually
439 inspected and downsampled to 200 Hz to increase the processing speed in later analyses[69].
440 *Sensor space analysis:* The baseline MEG signal for each trial was calculated by averaging
441 the signals during the 0.2-s period preceding the onset of the targeting period, and the

442 baseline was subtracted from the signal at each time point during the targeting period in that
443 trial. Then, the time series of the MEG signal was averaged across trials for each target and
444 control condition. Contrast analyses were performed to compare the difference between the
445 left/right-target and back-target conditions, and to test the effects of the recollection in each
446 of the three target conditions relative to the control conditions. These analyses were
447 performed on each sensor, and a sensor space was generated for each session. The sensor
448 spaces were averaged across sessions before submitting them to the statistical test for group-
449 level statistical analysis.
450 *Source space analysis:* To reconstruct the spatial-temporal activity from the sensor space to
451 the anatomical space, the forward model was created using a single-compartment (inner
452 skull) boundary-element method on the basis of each participant's anatomical image, and the
453 spatial-temporal activity was then inversely modeled using the dynamic statistical parameter
454 map at each source point and time[30]. The source space was estimated using a subsampling
455 strategy, which involved subdividing a polygon (oct6) using the spherical coordinate system
456 provided by FreeSurfer, producing 4098 source points per hemisphere with an average source
457 spacing of 4.9 mm (assuming a surface area of 1000 $cm^2$/hemisphere)[67,70]. The source space
458 of each participant was morphed to an average surface. The percentile ranks of source-power
459 strength from the top 5% to 1% was calculated for each egocentric location in comparison
460 with the control condition or the contrast between the left/right and back conditions. For ROI
461 analysis, we manually delineated each of the medial temporal lobe (MTL) subareas
462 (hippocampus [HPC], parahippocampal cortex [PHC], perirhinal cortex [PRC], and
463 entorhinal cortex [ERC]) on the participant's native space using established protocols[71-74] as
464 well as the delineating software ITK-SNAP (www.itksnap.org). The mean source power
465 within the MTL subareas was calculated by averaging the source power within each mask for
466 each egocentric location before submitting it to a group-level statistical analysis.

467 *Connectivity analysis:* To assess the connectivity of the parietal cortex and precuneus with
468 the frontal lobe (FEF/supplementary motor area [SMA]) and MTL subareas in each temporal
469 period revealed by the MEG contrast analysis (i.e., "early" [0.25–0.37 s after the onset of
470 targeting period] for the back-target condition and "late" [0.67–0.85 s] for the left/right-target
471 condition), we examined the phase synchronization of the MEG time series for the following
472 four frequency bands: alpha (8–13 Hz), beta (13–30 Hz), low-gamma (30–60 Hz), and high-
473 gamma (60–99 Hz) bands. For this purpose, we first calculated the powers of the MEG signal
474 in a time window of 400 ms centering iteratively at each of the time points within the two
475 time periods. The 400-ms time window was applied in this analysis to ensure that at least
476 three cycles of the source time series could be covered in the alpha band[75]. The powers at
477 each time point were averaged across trials including all target locations and a control
478 condition for each participant, and the grand-mean of power across participants was
479 calculated. We selected the centering time point of the time window that had the maximum
480 grand-mean power for each time period. This procedure yielded two time-series (the time
481 window of 0.08–0.48 s corresponding to the centering point of 0.28 s and the time window of
482 0.56–0.96 s corresponding to the centering point of 0.76 s for the "early" and "late" periods,
483 respectively). Phase synchronization was tested among the eight ROIs (parietal cortex,
484 precuneus, FEF, SMA, and right MTL subareas) for each time series, condition (left, right, or
485 back), and frequency band using PLI[31,32] and the built-in function of the MNE Python
486 toolbox[67,68]. In each frequency band, we calculated the difference in the connectivity of each
487 time series for each ROI between the back- and left/right-target conditions before group-level
488 statistical analysis.
489
490 **Statistical analysis**

For the MRI univariate and connectivity analyses, an initial threshold of $P < 0.01$ was applied to each voxel, and the reliability of clusters was tested using a nonparametric statistical inference that did not make assumptions about the distribution of the data[22,66,67]. The test was conducted with the FSL randomize package (version v2.9, http://fsl.fmrib.ox.ac.uk/fsl/fslwiki/Randomise) with 5000 random sign-flips, and clusters with a size higher than 95% of the maximal supra-threshold clusters in the permutation distribution were then reported. Data obtained by ROI analysis of the MRI BOLD signal, MEG source power, and MEG connectivity analysis were tested using either a *t*-test with Bonferroni correction or repeated-measures two-way ANOVA. The MEG sensor space analysis used either a spatial-temporal cluster permutation test or a spatial-cluster permutation test. All statistical tests were two-sided unless otherwise noted, and significance was determined when the corrected *P* value was less than 0.05.

**Data and code availability**

The datasets and code supporting the current study are available from the corresponding author (Yuji Naya, yujin@pku.edu.cn) upon reasonable request.

507 **References**


508 1. Stein JF (1989) Representation of egocentric space in the posterior parietal cortex. Q
509 J Exp Physiol 74:583–606.
510 2. Shelton AL, McNamara TP (1997) Multiple views of spatial memory. Psychon Bull Rev
511 4:102–106.
512 3. Burgess N (2006) Spatial memory: how egocentric and allocentric combine. Trends
513 Cogn Sci 10:551–557.
514 4. Crawford JD, Henriques DY, Medendorp WP (2011) Three-dimensional
515 transformations for goal-directed action. Annu Rev Neurosci 34:309–331.
516 5. Khan AZ, Blangero A, Rossetti Y, Salemme R, Luauté J, Deubel H, Schneider WX,
517 Laverdure N, Rode G, Boisson D, Pisella L (2009) Parietal damage dissociates saccade
518 planning from presaccadic perceptual facilitation. Cereb Cortex 19:383–387.
519 6. Ciaramelli E, Rosenbaum RS, Solcz S, Levine B, Moscovitch M (2010) Mental space
520 travel: damage to posterior parietal cortex prevents egocentric navigation and
521 reexperiencing of remote spatial memories. J Exp Psychol Learn Mem Cogn 36:619–
522 634.
523 7. Iriki A, Taoka M (2012) Triadic (ecological, neural, cognitive) niche construction: a
524 scenario of human brain evolution extrapolating tool use and language from the
525 control of reaching actions. Philos Trans R Soc Lond B Biol Sci 367:10–23.
526 8. Verhagen L, Dijkerman HC, Medendorp WP, Toni I (2013) Hierarchical organization of
527 parietofrontal circuits during goal-directed action. J Neurosci 33:6492–6503.
528 9. Wang X, Fung CC, Guan S, Wu S, Goldberg ME, Zhang M (2016) Perisaccadic
529 receptive field expansion in the lateral intraparietal area. Neuron 90:400–409.

530 10. Zhou Y, Liu Y, Lu H, Wu S, Zhang M (2016) Neuronal representation of saccadic error
531 in macaque posterior parietal cortex (PPC). eLife 5:e10912.
532 11. Goodale MA, Milner AD (1992) Separate visual pathways for perception and action.
533 Trends Neurosci 15:20–25.
534 12. Ungerleider LG, Pessoa L (2008) What and where pathways. Scholarpedia 3:5342.
535 13. Stein JF (1992) The representation of egocentric space in the posterior parietal
536 cortex. Behav Brain Sci 15 Spec No 4:691–700.
537 14. Desmurget M, Epstein CM, Turner RS, Prablanc C, Alexander GE, Grafton ST (1999)
538 Role of the posterior parietal cortex in updating reaching movements to a visual
539 target. Nat Neurosci 2:563–567.
540 15. Donner T, Kettermann A, Diesch E, Ostendorf F, Villringer A, Brandt SA (2000)
541 Involvement of the human frontal eye field and multiple parietal areas in covert
542 visual selection during conjunction search. Eur J Neurosci 12:3407–3414.
543 16. Bisley JW, Mirpour K (2019) The neural instantiation of a priority map. Curr Opin
544 Psychol 29:108–112.
545 17. Vallar G (1998) Spatial hemineglect in humans. Trends Cogn Sci 2:87–97.
546 18. Bisiach E, Luzzatti C (1978) Unilateral neglect of representational space. Cortex
547 14:129–133.
548 19. Farrer C, Frith CD (2002) Experiencing oneself vs another person as being the cause
549 of an action: the neural correlates of the experience of agency. Neuroimage 15:596–
550 603.
551 20. Spiers HJ, Maguire EA (2007) A navigational guidance system in the human brain.
552 Hippocampus 17:618–626.

553 21. Gaesser B, Spreng RN, McLelland VC, Addis DR, Schacter DL (2013) Imagining the
554 future: evidence for a hippocampal contribution to constructive processing.
555 Hippocampus 23:1150–1161.
556 22. Chadwick MJ, Jolly AE, Amos DP, Hassabis D, Spiers HJ (2015) A goal direction signal
557 in the human entorhinal/subicular region. Curr Biol 25:87–92.
558 23. Suarez-Jimenez B, Bisby JA, Horner AJ, King JA, Pine DS, Burgess N (2018) Linked
559 networks for learning and expressing location-specific threat. Proc Natl Acad Sci U S
560 A 115:E1032–E1040.
561 24. Attneave F, Farrar P (1977) The visual world behind the head. Am J Psychol 90:549–
562 563.
563 25. Sholl MJ (1987) Cognitive maps as orienting schemata. J Exp Psychol Learn Mem
564 Cogn 13:615–628.
565 26. Presson CC, Hazelrigg MD (1984) Building spatial representations through primary
566 and secondary learning. J Exp Psychol Learn Mem Cogn 10:716–722.
567 27. Kelly JW, McNamara TP (2009) Facilitated pointing to remembered objects in front:
568 evidence for egocentric retrieval or for spatial priming? Psychon Bull Rev 16:295–
569 300.
570 28. Schindler A, Bartels A (2013) Parietal cortex codes for egocentric space beyond the
571 field of view. Curr Biol 23:177–182.
572 29. Zhang B, Naya Y (2020) Medial prefrontal cortex represents the object-based
573 cognitive map when remembering an egocentric target location. Cereb Cortex
574 30:5356–5371.

575 30. Dale AM, Liu AK, Fischl BR, Buckner RL, Belliveau JW, Lewine JD, Halgren E (2000)
576 Dynamic statistical parametric mapping: combining fMRI and MEG for high-
577 resolution imaging of cortical activity. Neuron 26:55–67.
578 31. Stam CJ, Nolte G, Daffertshofer A (2007) Phase lag index: assessment of functional
579 connectivity from multi channel EEG and MEG with diminished bias from common
580 sources. Hum Brain Mapp 28:1178–1193.
581 32. Colclough GL, Woolrich MW, Tewarie PK, Brookes MJ, Quinn AJ, Smith SM (2016)
582 How reliable are MEG resting-state connectivity metrics? Neuroimage 138:284–293.
583 33. Schacter DL, Addis DR, Buckner RL (2007) Remembering the past to imagine the
584 future: the prospective brain. Nat Rev Neurosci 8:657–661.
585 34. Byrne P, Becker S, Burgess N (2007) Remembering the past and imagining the future:
586 a neural model of spatial memory and imagery. Psychol Rev 114:340–375.
587 35. Grave de Peralta-Menendez RG, Gonzalez-Andino SL (1998) A critical analysis of
588 linear inverse solutions to the neuroelectromagnetic inverse problem. IEEE Trans Bio
589 Med Eng 45:440–448.
590 36. Sato MA, Yoshioka T, Kajihara S, Toyama K, Goda N, Doya K, Kawato M (2004)
591 Hierarchical Bayesian estimation for MEG inverse problem. Neuroimage 23:806–826.
592 37. Colclough GL, Brookes MJ, Smith SM, Woolrich MW (2015) A symmetric multivariate
593 leakage correction for MEG connectomes. Neuroimage 117:439–448.
594 38. Logothetis NK, Pauls J, Augath M, Trinath T, Oeltermann A (2001) Neurophysiological
595 investigation of the basis of the fMRI signal. Nature 412:150–157.
596 39. Hafting T, Fyhn M, Molden S, Moser MB, Moser EI (2005) Microstructure of a spatial
597 map in the entorhinal cortex. Nature 436:801–806.

598 40. Hargreaves EL, Rao G, Lee I, Knierim JJ (2005) Major dissociation between medial
599 and lateral entorhinal input to dorsal hippocampus. Science 308:1792–1794.
600 41. Howard LR, Javadi AH, Yu Y, Mill RD, Morrison LC, Knight R, Loftus MM, Staskute L,
601 Spiers HJ (2014) The hippocampus and entorhinal cortex encode the path and
602 Euclidean distances to goals during navigation. Curr Biol 24:1331–1340.
603 42. Wang C, Chen X, Lee H, Deshmukh SS, Yoganarasimha D, Savelli F, Knierim JJ
604 (2018) Egocentric coding of external items in the lateral entorhinal cortex. Science
605 362:945–949.
606 43. Doeller CF, Barry C, Burgess N (2010) Evidence for grid cells in a human memory
607 network. Nature 463:657–661.
608 44. Killian NJ, Jutras MJ, Buffalo EA (2012) A map of visual space in the primate
609 entorhinal cortex. Nature 491:761–764.
610 45. Wilming N, König P, König S, Buffalo EA (2018) Entorhinal cortex receptive fields are
611 modulated by spatial attention, even without movement. eLife 7:e31745.
612 46. Horner AJ, Bisby JA, Zotow E, Bush D, Burgess N (2016) Grid-like processing of
613 imagined navigation. Curr Biol 26:842–847.
614 47. Tambini A, Nee DE, D'Esposito M (2018) Hippocampal-targeted theta-burst
615 stimulation enhances associative memory formation. J Cogn Neurosci 30:1452–1472.
616 48. Tambini A, Davachi L (2019) Awake reactivation of prior experiences consolidates
617 memories and biases cognition. Trends Cogn Sci 23:876–890.
618 49. Yang C, Naya Y (2020) Hippocampal cells integrate past memory and present
619 perception for the future. PLOS Biol 18:e3000876.

620 50. Doesburg SM, Green JJ, McDonald JJ, Ward LM (2009) From local inhibition to long-
621 range integration: a functional dissociation of alpha-band synchronization across
622 cortical scales in visuospatial attention. Brain Res 1303:97–110.
623 51. Sadaghiani S, Scheeringa R, Lehongre K, Morillon B, Giraud AL, D'Esposito M,
624 Kleinschmidt A (2012) Alpha-band phase synchrony is related to activity in the
625 fronto-parietal adaptive control network. J Neurosci 32:14305–14310.
626 52. Takahashi T, Kitazawa S (2017) Modulation of illusory reversal in tactile temporal
627 order by the phase of posterior α rhythm. J Neurosci 37:5298–5308.
628 53. Lobier M, Palva JM, Palva S (2018) High-alpha band synchronization across frontal,
629 parietal and visual cortex mediates behavioral and neuronal effects of visuospatial
630 attention. Neuroimage 165:222–237.
631 54. Chen H, Naya Y (2020a) Forward processing of object–location association from the
632 ventral stream to medial temporal lobe in nonhuman primates. Cereb Cortex
633 30:1260–1271.
634 55. Chen H, Naya Y (2020b) Automatic encoding of a view-centered background image in
635 the macaque temporal lobe. Cereb Cortex 30:6270–6283.
636 56. Naya Y, Suzuki WA (2011) Integrating what and when across the primate medial
637 temporal lobe. Science 333:773–776.
638 57. Eichenbaum H, Cohen NJ (2014) Can we reconcile the declarative memory and
639 spatial navigation views on hippocampal function? Neuron 83:764–770.
640 58. Woolrich MW, Ripley BD, Brady M, Smith SM (2001) Temporal autocorrelation in
641 univariate linear modeling of FMRI data. NeuroImage 14:1370–1386.
642

643 59. Woolrich MW, Behrens TEJ, Smith SM (2004) Constrained linear basis sets for HRF
644 modelling using Variational Bayes. NeuroImage 21:1748–1761.
645 60. Jenkinson M, Smith S (2001) A global optimisation method for robust affine
646 registration of brain images. Med Image Anal 5:143–156.
647 61. Jenkinson M, Bannister P, Brady M, Smith S (2002) Improved optimization for the
648 robust and accurate linear registration and motion correction of brain images.
649 Neuroimage 17:825–841.
650 62. Fox MD, Snyder AZ, Vincent JL, Corbetta M, Van Essen DC, Raichle ME (2005) The
651 human brain is intrinsically organized into dynamic, anticorrelated functional
652 networks. Proc Natl Acad Sci U S A 102:9673–9678.
653 63. Vincent JL, Snyder AZ, Fox MD, Shannon BJ, Andrews JR, Raichle ME, Buckner RL
654 (2006) Coherent spontaneous activity identifies a hippocampal-parietal memory
655 network. J Neurophysiol 96:3517–3531.
656 64. Tompary A, Davachi L (2017) Consolidation promotes the emergence of
657 representational overlap in the hippocampus and medial prefrontal cortex. Neuron
658 96:228–241.e5.
659 65. Rolls ET, Joliot M, Tzourio-Mazoyer N (2015) Implementation of a new parcellation of
660 the orbitofrontal cortex in the automated anatomical labeling atlas. Neuroimage
661 122:1–5.
662 66. Ranganath C, Heller A, Cohen MX, Brozinsky CJ, Rissman J (2005) Functional
663 connectivity with the hippocampus during successful memory formation.
664 Hippocampus 15:997–1005.

67. Gramfort A, Luessi M, Larson E, Engemann DA, Strohmeier D, Brodbeck C, Goj R, Jas M, Brooks T, Parkkonen L, Hämäläinen M (2013) MEG and EEG data analysis with MNE-Python. Front Neurosci 7:267.

68. Gramfort A, Luessi M, Larson E, Engemann DA, Strohmeier D, Brodbeck C, Parkkonen L, Hämäläinen MS (2014) MNE software for processing MEG and EEG data. Neuroimage 86:446–460.

69. Grenander U (1959) Probability and Statistics: the Harald Cramér Volume. New York, NY: Almqvist & Wiksell.

70. Fischl B, Sereno MI, Tootell RB, Dale AM (1999) High-resolution intersubject averaging and a coordinate system for the cortical surface. Hum Brain Mapp 8:272–284.

71. Duvernoy HM (2005) The Human Hippocampus: Functional Anatomy, Vascularization and Serial Sections with MRI. New York, NY: Springer Science and Business Media.

72. Insausti R, Juottonen K, Soininen H, Insausti AM, Partanen K, Vainio P, Laakso MP, Pitkänen A (1998) MR volumetric analysis of the human entorhinal, perirhinal, and temporopolar cortices. AJNR Am J Neuroradiol 19:659–671.

73. Pruessner JC, Li LM, Serles W, Pruessner M, Collins DL, Kabani N, Lupien S, Evans AC (2000) Volumetry of hippocampus and amygdala with high-resolution MRI and three-dimensional analysis software: minimizing the discrepancies between laboratories. Cereb Cortex 10:433–442.

74. Pruessner JC, Köhler S, Crane J, Pruessner M, Lord C, Byrne A, Kabani N, Collins DL, Evans AC (2002) Volumetry of temporopolar, perirhinal, entorhinal and parahippocampal cortex from high-resolution MR images: considering the variability of the collateral sulcus. Cereb Cortex 12:1342–1353.

75. Hu L, Zhang Z (2019) EEG Signal Processing and Feature Extraction. Singapore: Springer Singapore.

76. Nichols TE, Holmes AP (2002) Nonparametric permutation tests for functional neuroimaging: a primer with examples. Hum Brain Mapp 15:1–25.

77. Winkler AM, Ridgway GR, Webster MA, Smith SM, Nichols TE (2014) Permutation inference for the general linear model. Neuroimage 92:381–397.

695 **Figures**

696

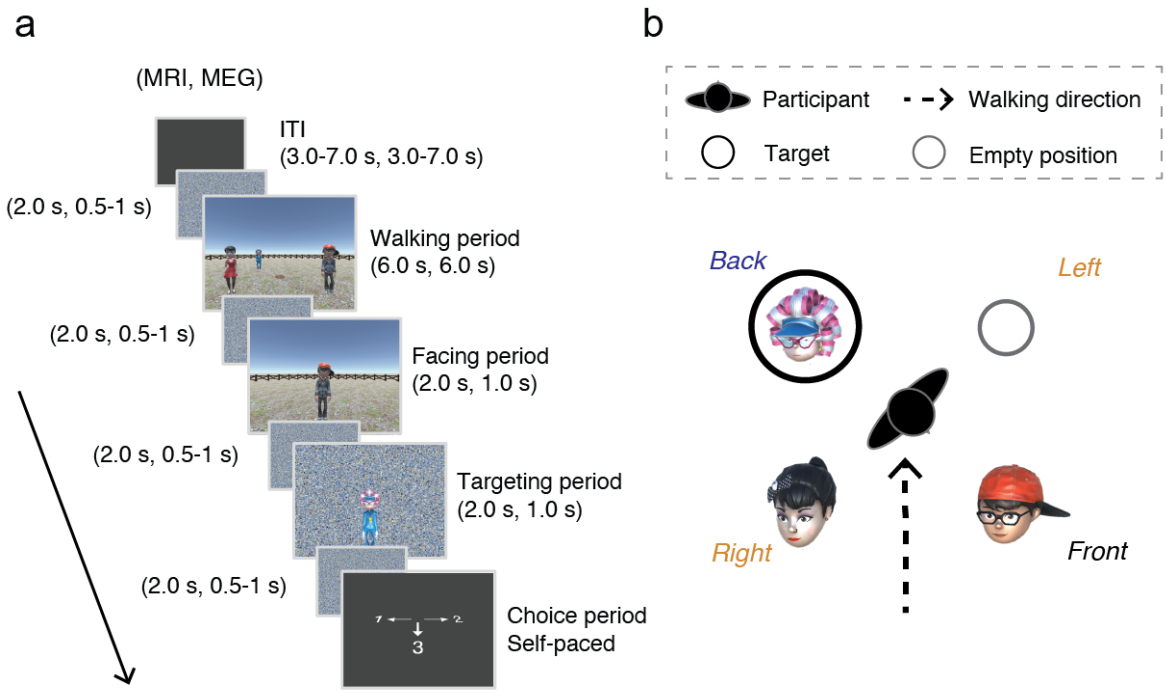


697

698 Figure 1. a) Spatial-memory task paradigm. Each trial consisted of four periods. Walking
699 period: participants walked toward three human characters using the first-person perspective
700 and stopped on a wood plate in the center. Facing period: one of the human characters was
701 presented, indicating the participant's current self-orientation. Targeting period: a photo of
702 the target character was presented on a scrambled background. Choice period: the
703 participants chose the direction of the target character relative to their body upon the
704 presentation of a response cue. b) The spatial relationship between the participant and the
705 human characters in the example trial of Fig. 1a, with the target location behind the
706 participant's self-body (*black circle*).

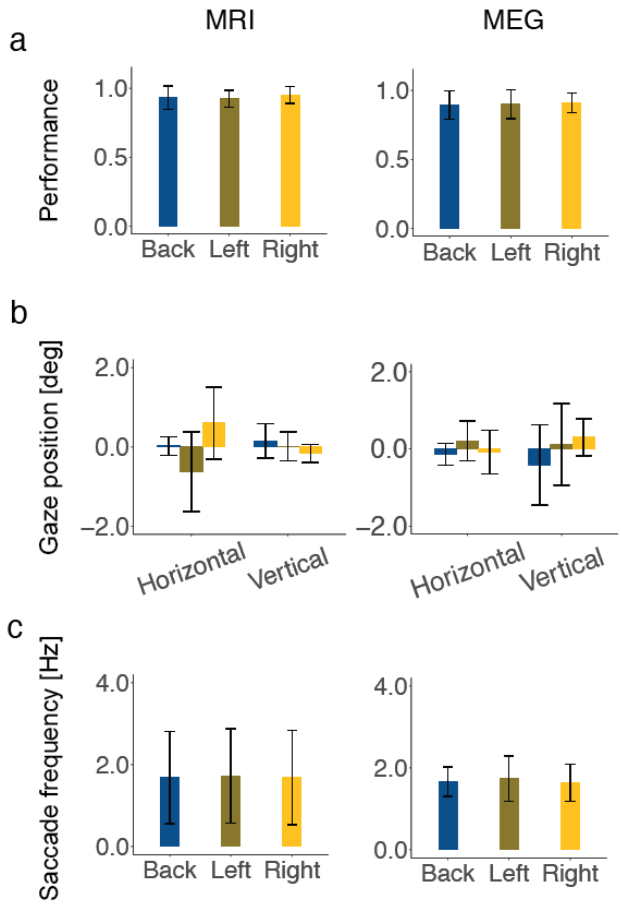


Figure 2. a) Performance of participants for the three egocentric target locations in the MRI (n = 19) and MEG (n = 12) experiments. A statistically significant difference was not detected in the performances of the target locations by repeated-measures one-way ANOVA in the MRI [$F(2,54) = 0.82$, $P = 0.44$] or MEG [$F(2,33) = 0.08$, $P = 0.93$] experiments. b) Gaze positions of the participants during the targeting period (4 s for MRI, 1 s for MEG) were shown for each target condition. No significant difference was found among the left, right, and back-target conditions in the MRI experiments [horizontal: $F(2, 51) = 1.7$, $P = 0.19$, vertical: $F(2, 51) = 0.08$, P = 0.92) or the MEG experiments [horizontal: $F(2, 27) = 0.32$, $P = 0.73$, vertical: $F(2, 27) = 0.42$, $P = 0.66$]. c) No significant difference in the frequencies of saccadic eye movements was found among the three conditions during the targeting period [MRI: $F(2, 51) = 0.01$, $P = 0.99$; MEG: $F(2, 27) = 0.14$, $P = 0.87$]. Error bars indicate standard deviations.

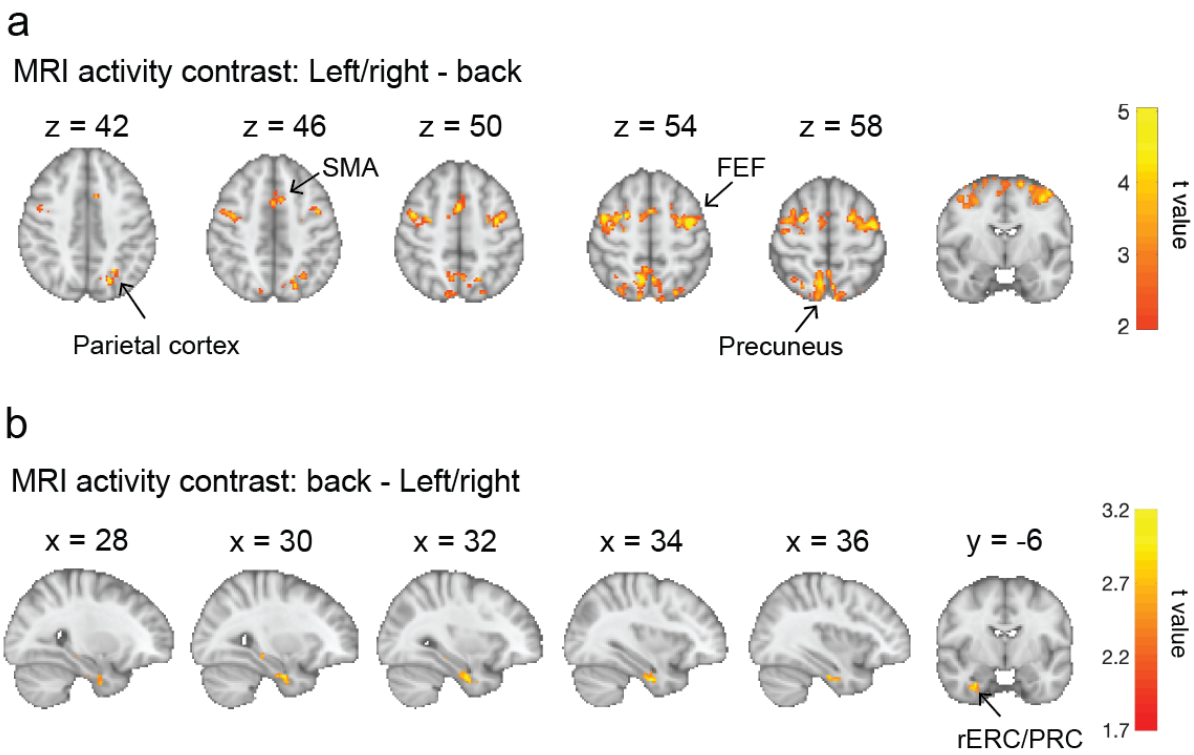


721

722 Figure 3. a) MRI contrast for the "left/right-target" – "back-target" condition: significant

723 clusters were observed in the parietal cortex, precuneus, FEF, and SMA ($P < 0.01$, initial

724 threshold, $P < 0.05$, cluster-corrected for multiple comparison). b) MRI contrast for the

725 "back-target" – "left/right-target" condition: a cluster was observed in the right rhinal cortex,

726 including the entorhinal cortex (ERC) and perirhinal cortex (PRC) ($P < 0.05$ uncorrected).

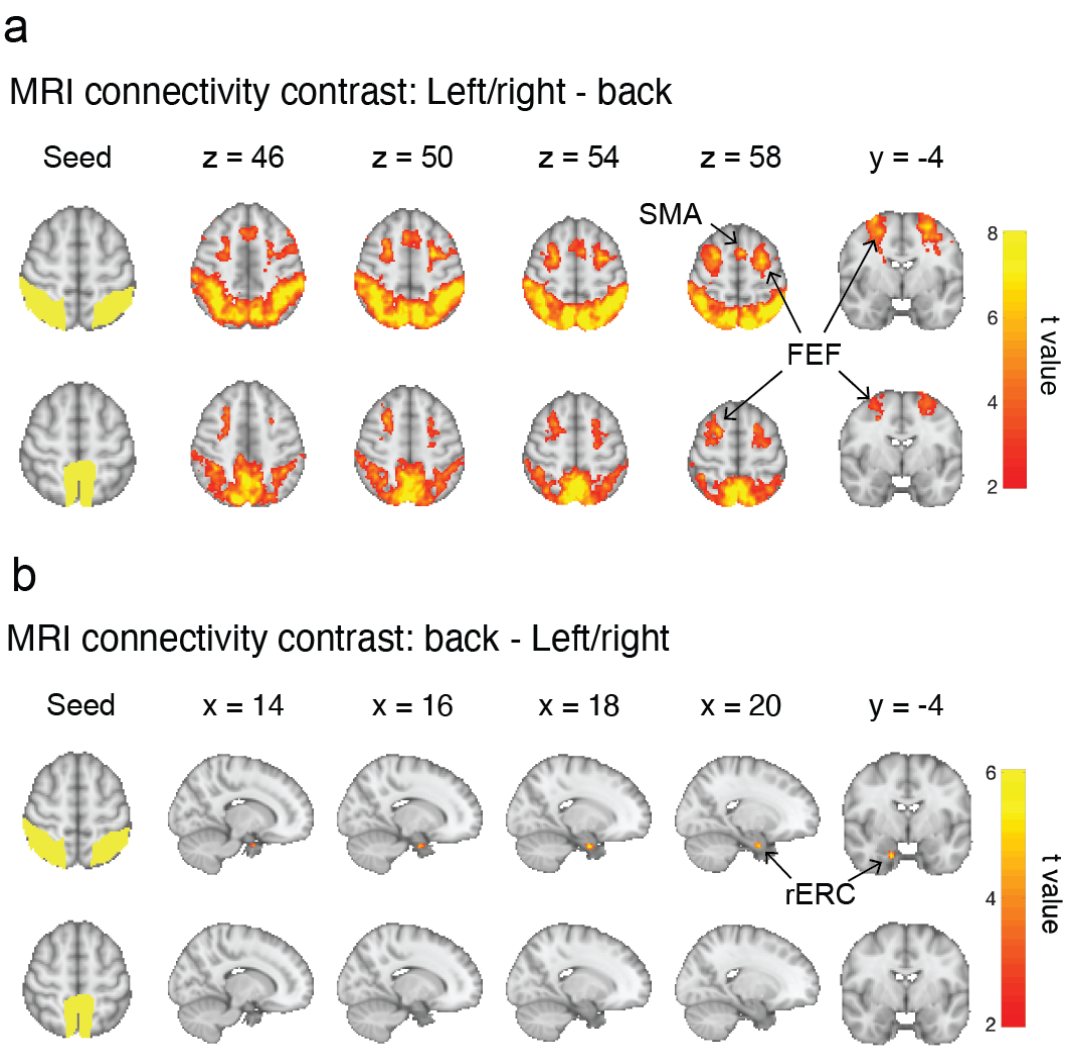


Figure 4. MRI connectivity analysis using the parietal cortex and precuneus as seeds. a) Connectivity contrast for the "left/right-target" – "back-target" condition: significant connections were found in the parietal cortex, precuneus, FEF, and SMA for both seeds ($P < 0.01$, initial threshold, $P < 0.05$, cluster-corrected for multiple comparison). b) Connectivity contrast for the "back-target" – "left/right-target" condition: a significant connection was observed between the parietal cortex and right ERC ($P < 0.01$, initial threshold, $P < 0.05$, cluster-corrected for multiple comparisons via small-volume correction using the bilateral MTL mask); no connection was found between the precuneus and MTL regions.

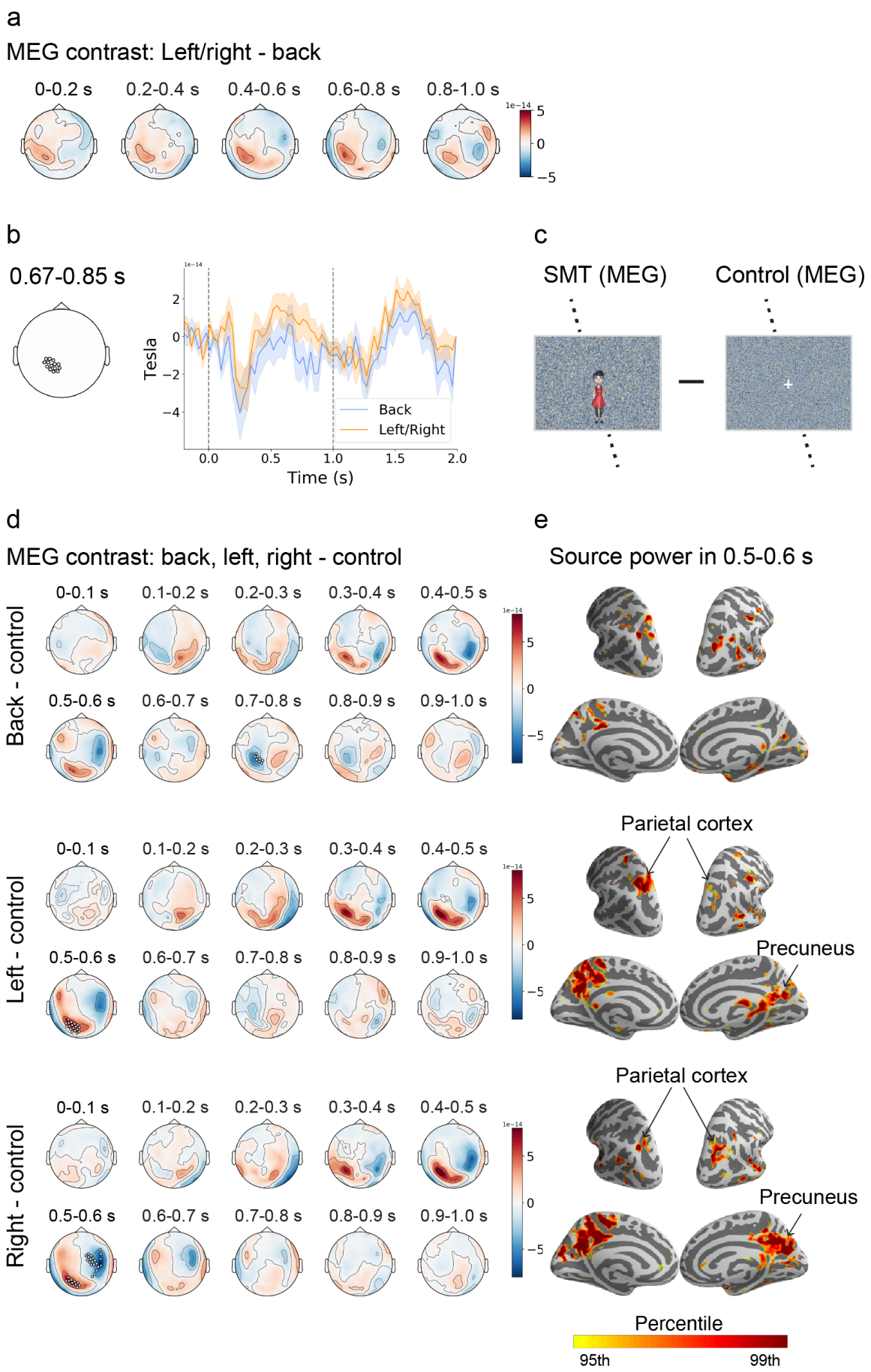
a
MEG contrast: Left/right - back
0-0.2 s
0.2-0.4 s
0.4-0.6 s
0.6-0.8 s
0.8-1.0 s
1e−14
5
0
−5
b
0.67-0.85 s
Tesla
Time (s)
Back
Left/Right
c
SMT (MEG)
Control (MEG)
d
MEG contrast: back, left, right - control
Back - control
Left - control
Right - control
0-0.1 s
0.1-0.2 s
0.2-0.3 s
0.3-0.4 s
0.4-0.5 s
0.5-0.6 s
0.6-0.7 s
0.7-0.8 s
0.8-0.9 s
0.9-1.0 s
e
Source power in 0.5-0.6 s
Parietal cortex
Precuneus
Percentile
95th
99th

Figure 5. a) Mean topographic map for the MEG contrast of "left/right-target" – "back-target" condition for every 0.2 s during the targeting period. b) Time courses of the signal strength on the left-posterior cluster of sensors in the back-target and left/right-target conditions. A significantly higher activity was found for the left/right-target condition relative to the back-target condition during 0.67–0.85 s after the onset of the targeting period ($P < 0.05$, initial threshold, $P < 0.05$, spatial-temporal cluster correction for multiple comparison, two tailed). c) A comparison between the spatial-memory-task (SMT) trials and the control-condition trials in the MEG experiment. d) Mean topographic map for the left-target, right-target, and back-target conditions relative to the control condition for every 0.1 s during the targeting period. Significant clusters were found in the left-posterior from 0.5 to 0.6 s for the left-target and right-target conditions ($P < 0.05$, initial threshold; $P < 0.05$, cluster-corrected for multiple comparison, two tailed), but not for the back-target condition. e) Source-power distribution on the brain surface for each of the three conditions relative to the control condition within 0.5–0.6 s. Color bar represents the percentile rank of source-power strength.

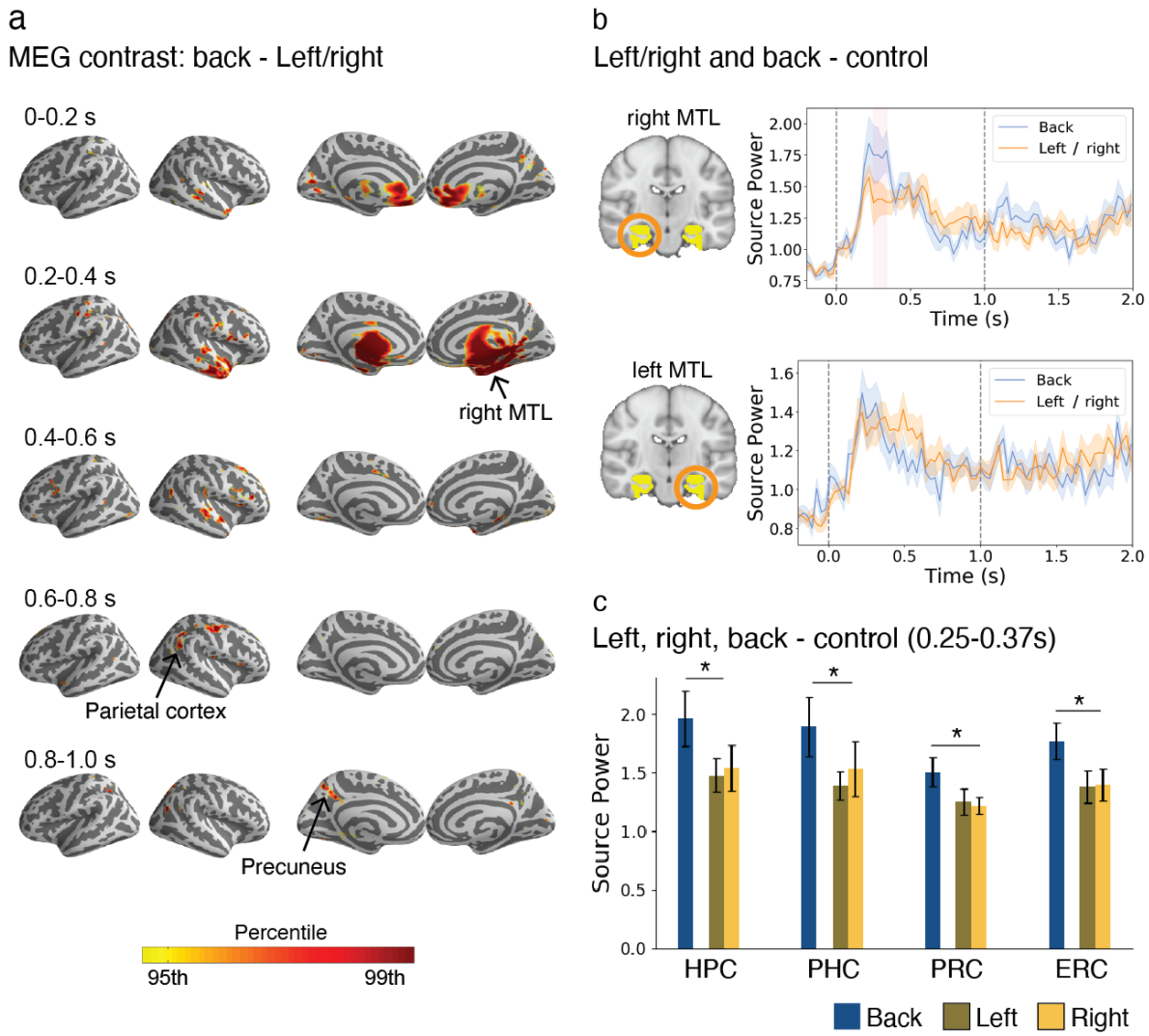


754

755 Figure 6. a) MEG contrast for the "back-target" – "left/right-target" condition in source-
756 power for every 0.2 s during the targeting period. The color bar represents the percentile rank
757 of source-power strength. b) Time courses of the source-power in the anatomical ROIs for
758 both hemispheres of the MTL. The shaded area (right MTL, 0.25–0.37 s after the onset of
759 targeting period in the top panel) indicates a significantly higher source-power in the back-
760 target condition than in the left/right-target condition ($P < 0.05$, spatial-temporal cluster
761 correction for multiple comparison, two tailed). c) ROI analysis of the source-power in each
762 of the right MTL subregions for each condition. *$P < 0.05$, $t$ (11) = 3.00, 2.98, 3.22, and 3.39
763 for HPC, PHC, PRC, and ERC, respectively, "back" vs. "left/right," two-tailed, Bonferroni-
764 corrected for multiple comparisons (n = 4). Error bars represent SEMs.

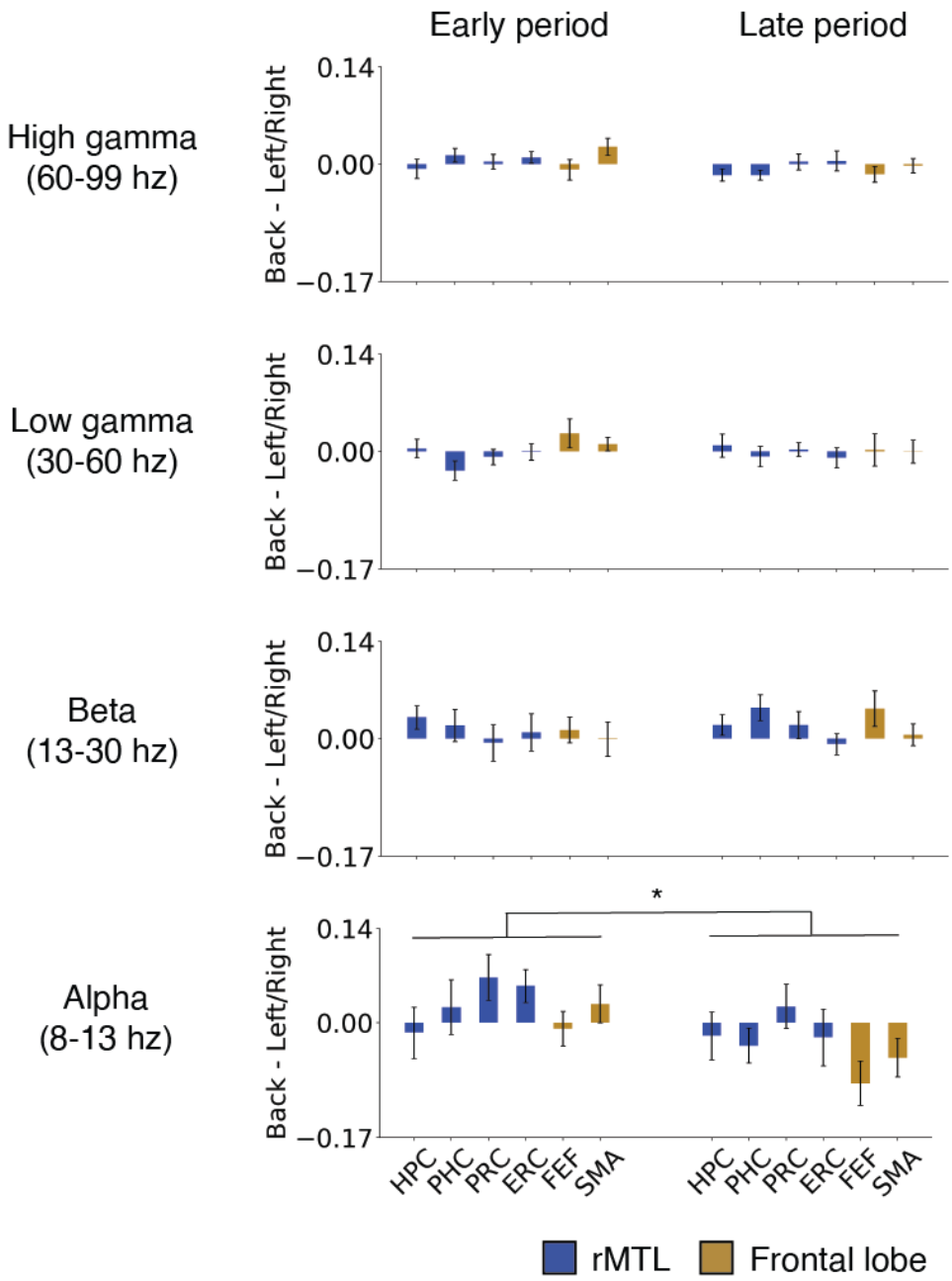


Figure 7. MEG connectivity contrast for the "back-target" – "left/right-target" condition using the parietal cortex as a seed. The connectivity with each of the six anatomical ROIs was estimated for alpha, beta, and gamma frequency bands using PLI during the early phase (0.08–0.48 s) and late phase (0.56–0.96 s). *$P$ = 0.02, $F$ (2, 132) = 8.24, a main effect of time-windows (early vs. late), repeated-measures two-way ANOVA with brain areas as another main effect, Bonferroni-corrected for multiple comparisons of frequency bands (n = 4). Error bars represent SEMs.